Polymer Bulletin 60, 495–505 (2008)
DOI 10.1007/s00289-008-0887-9

Polymer Bulletin

Preparation and characterization of poly(methyl methacrylate) nanocomposites containing octavinyl polyhedral oligomeric silsesquioxane

Chunbao Zhao[1,2], Xujie Yang[1] (✉), Xiaodong Wu[1], Xiaoheng Liu[1], Xin Wang[1], Lude Lu[1]

[1] Materials Chemistry Laboratory, Nanjing University of Science and Technology, Nanjing, Jiangsu 210094, P.R. China
[2] Nanjing College of Information and Technology, Nanjing, Jiangsu 210046, P.R. China
E-mail: yangxj2000@yahoo.com.cn; Fax: +86 25 84315054

Received: 11 July 2007 / Revised version: 20 December 2007 / Accepted: 21 December 2007
Published online: 12 January 2008 –

Summary

A series of poly(methyl methacrylate) (PMMA) containing octavinyl-polyhedral oligomeric silsesquioxane (OV-POSS) nanocomposites were synthesized by solution polymerization. The products were characterized by FTIR, ^{1}H NMR, GPC, TEM, DSC and TGA. The actual contents of OV-POSS in the obtained products and the reaction degree of the vinyl groups in the POSS were calculated on the basis of FTIR, TGA and ^{1}H NMR data respectively. The DSC and TGA results indicate that the incorporation of POSS molecules could improve the thermal properties of PMMA nanocomposites significantly. The glass transition temperature (T_g) and thermal decomposition temperature (T_{dec1}) of the nanocomposite with 12.27 wt % of OV-POSS were increased by 23°C and 93°C correspondingly. In our experiment, the improved thermal properties were largely attributed to the nanoreinforcement effect of POSS cages and the formation of star-shaped structures with cubic silsesquioxane core.

Introduction

Polymer/inorganic nanocomposites that combine the advantages of inorganic and organic materials often exhibit unexpectedly improved properties [1-5]. The properties of polymer composites depend on the type of incorporated nanoparticles, their size and shape, their concentration and interactions with the polymer matrix [6-9]. During the last decade, many nanosized clusters involving clay layered silicates [6,10,11], zirconia [7], carbon nanotubes [8,12] have been developed to prepare polymer/inorganic hybrids.

Recently, polyhedral oligomeric silsesquioxanes (POSS) have attracted considerable attention as molecular silica and nano-scaled building blocks for preparing nanocomposites [13-21]. POSS is a special hybrid compound which possess a well-defined cage-like core, that is externally covered by organic substituents [22]. The type and number of the substituents can be varied by molecular design. Therefore, POSS moieties can be readily incorporated into polymer matrices to prepare new

hybrid nanocomposites with remarkable enhancements in mechanical and physical properties, including dramatic increases in use temperatures [13,23], oxidation resistance [14], and moduli [24], reduced flammability [15,25], and heat evolution [16]. Poly(methyl methacrylate) is an important thermoplastic with excellent transparency, high moduli, and relative ease of processing. However, its application is limited at elevated temperature because of its relatively poor thermal stability. It has been proved that a available way to solve this problem is to prepare organic/inorganic nanocomposites by incorporating nano-sized inorganic components into polymeric matrices by physical blending. Nanocomposites of PMMA containing clay layered silicates, zirconia, silica, titania and mixture of silica/zirconia nanoparticles, respectively, have exhibited enhancement in thermal and mechanical properties [6,7,26-28]. However, it is difficult for physical blending to disperse the particles into polymer uniformly. In recent years, some researchers are shifting their interests toward the synthesis of POSS-containing hybrid PMMA composites. A variety of PMMA/POSS nanocomposites have been prepared through the physical blending [29-32], copolymerization [33-36] and atom transfer radical polymerization (ATRP) technique [37-40]. In light of the recent work on PMMA/POSS nanocomposites, the thermal properties of composites are strongly influenced by the type of POSS and the preparation methods of composites. Kopesky et al. [29] investigated the miscibility and viscoelastic properties of acrylic-POSS/PMMA blends and found that POSS species can lead to lower the glass transition temperature. Similar results were also obtained by them in another work [30]. Weickmann and his coworkers [31] reported novel PMMA/POSS composites prepared by self-assembly methodology. Though the toughness was enhanced, the POSS species failed to improve thermal properties. In contrast to nanocomposites prepared by physical blending, copolymers containing tethered POSS often exhibit enhanced thermal properties [33,41,42]. Toepfer et al. [33] used methacryloxypropyl-POSS to prepare cross-linked PMMA nanocomposites. In comparison with the pure PMMA, they obtained significant improvement in the thermal degradation temperatures and glass transition temperatures of the hybrids.

In this manuscript, octavinyl polyhedral oligomeric silsesquioxane was synthesized, characterized and used to prepare PMMA/POSS hybrid composites. The structure and morphology of these nanocomposites were determined by Fourier transform infrared (FTIR), nuclear magnetic resonance spectroscopy (NMR), gel permeation chromatography (GPC) and transmission electron microscopy (TEM). The thermal properties of the PMMA/OV-POSS nanocomposites were studied by differential scanning calorimetry (DSC) and thermogravimetric analysis (TGA), in a tempt to probe the effect of POSS on the thermal properties.

Experiment

Materials

Methyl methacrylate (MMA), azobis-(isobutyronitrile) (AIBN), tetrahydrofuran (THF), and 1,4-dioxane were of analytical grade, obtained from Shanghai Chemical Reagents Co., Shanghai, China. MMA monomer was distilled from calcium hydride under reduced pressure and stored in a refrigerator. AIBN was refined in heated ethanol and kept in a dried box. THF and 1,4-dioxane were dried over 4Å molecular sieves for 2 days and then distilled immediately before use. All other solvents were used as received.

Preparation of OV-POSS monomer and its nanocomposites

Octavinyl polyhedral oligomeric silsesquioxane was prepared according to Ref.[43]. The obtained product is white crystalline powder and the yield is 17.5%.
FTIR (KBr, cm^{-1}): νC=C (1604), δC-H (1410, 1277), νSi-O-Si (1099, 585). ^{1}H NMR ($CDCl_3$, ppm): 5.8~6.2 (m, 24H). ^{13}C NMR ($CDCl_3$, ppm): 131.3 (*C*H of vinyl), 139.6 (*C*H_2 of vinyl). ^{29}Si NMR ($CDCl_3$, ppm): -87. Elemental Analysis (%) found (cal.): C 30.24(30.33), H 3.61 (3.79).
PMMA/OV-POSS nanocomposites were prepared by solution polymerization, as shown in Scheme 1. Typically, in a 50 mL round-bottomed flask equipped with magnetic stirrer, thermometer, and reflux condenser, OV-POSS (0.125 g, 0.197 mmol), 1,4-dioxane (10 mL) , MMA monomer (2.375 g, 23.75 mmol), and AIBN (1 wt % in relative to based on monomer) were loaded under nitrogen atmosphere to produce the MMA/OV-POSS copolymers. The reaction mixture was stirred under nitrogen atmosphere at 69°C. After 8 h, the product was poured into excessive cyclohexane under vigorous agitation to dissolve the unreacted monomers and precipitate the nanocomposite. The crude product was redissolved in THF and precipitated in cyclohexane twice to remove the unreacted POSS and MMA monomers thoroughly. The solvent was removed in vacuo yielding the product as a white powder (yield, 70.6%) fully soluble in THF, $CHCl_3$ and Acetone. The contents of POSS in the nanocomposites were controlled to be 1, 5, 10, 15 and 20 wt %, respectively. For comparison, pure PMMA sample was produced with the same method as used for preparing the nanocomposites.

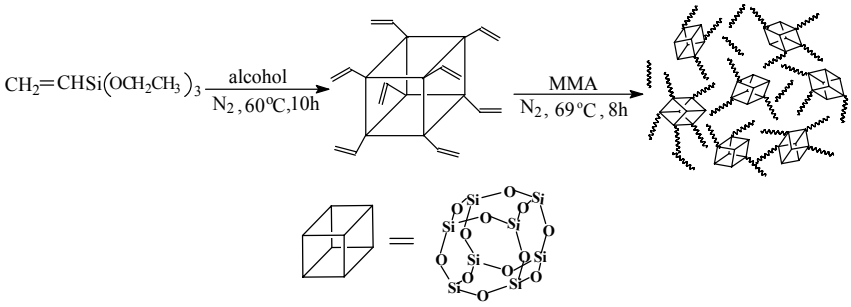

Scheme 1. Synthesis procedure of PMMA/OV-POSS nanocomposites

Characterizations

FTIR spectra were obtained with a Bruker Vector 22 instrument using KBr pellet at room temperature. Elemental analyses were measured with Vario EL Ⅲ automatic elemental analyzer. The ^{1}H NMR, ^{13}C NMR and ^{29}Si NMR measurements were conducted on a Bruker AVANCE 300 spectrometer at room temperature; deuterated chloroform was used as the solvent. The molecular weights and polydispersity index of the polymers were determined by a Waters Breeze HPLC gel permeation chromatography instrument, using polystyrene as the standard, and THF as the eluent at a flow rate of 1 mL·min^{-1}. DSC measurements were carried out on a METTLER TOLEDO DSC 823^{e} differential scanning calorimeter operated at a scan rate of 10°C·min^{-1} within a temperature range from 50 to 200°C under nitrogen flow. Thermal stabilities of the nanocoposites were evaluated on a METTLER TOLEDO

TGA/SDTA 851^e thermogravimetric analyzer at a heating rate of 20°C·min^{-1}. The thermal degradation temperatures (T_{dec1} and T_{dec2}) were defined as the onset temperature of 5 wt% and 10 wt% weight loss respectively. TEM was performed on a JEOL JEM-2100 high resolution transmission electron microscopy at an accelerating voltage of 200 kV.

Results and discussion

Preparation and structural characterization of the PMMA/POSS nanocomposites

Figure 1 displays the FTIR spectra of OV-POSS, pure PMMA and the PMMA/OV-POSS nanocomposites. The OV-POSS shows two characteristic absorptions at 1099 cm^{-1} and 585 cm^{-1}, which are assigned to Si-O-Si stretching and bending vibration, respectively. In the FTIR spectrum of pure PMMA, the band at 1731 cm^{-1} arises from the carbonyl stretching vibration of PMMA. The methyl and methylene groups exhibit absorption bands at ~3000 cm^{-1}. In the FTIR spectrum of the nanocomposites, the band at 585 cm^{-1} is present, and its intensity increases gradually with the increase of the concentration of OV-POSS, suggesting that the POSS cube structure is chemically incorporated into the hybrid nanocomposites.

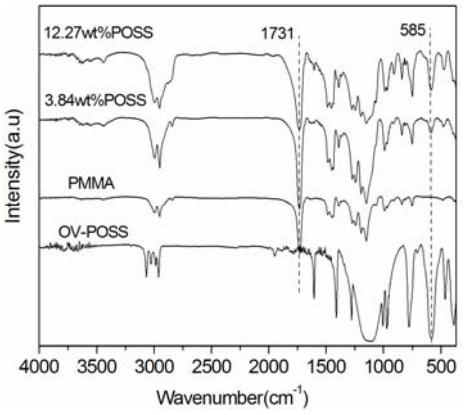

Figure 1. FTIR spectra of POSS, pure PMMA, and PMMA/POSS nanocomposites

FTIR spectroscopy is useful for determining the POSS content in POSS-containing copolymers [42,44]. For the PMMA/OV-POSS nanocomposites, the typical characteristic absorption peaks of PMMA and OV-POSS, without any overlapping with other peaks, locate at 1731 and 585 cm^{-1} respectively. A series of PMMA/OV-POSS blends with known quantities of OV-POSS and PMMA were prepared to obtain a standard calibration curve. OV-POSS and PMMA were, at first, dissolved in $CHCl_3$ to get a intimate mixture, followed by casting into a thin film on KBr pellet for FTIR analysis. The carbonyl band at 1731 cm^{-1} was taken as the internal standard. The ratios of area of the absorption bands (A_{585}/A_{1731}) were plotted against the weight percentage of POSS. The linear least square fit of the data gives a good calibration curve (shown in Figure 2) with the equation $X_{poss}=98.912A_{585}/A_{1731}+0.034$, where A_{585}/A_{1731} is the relative ratio of areas of the corresponding absorption bands and X_{poss} is the weight percentage of POSS in the blends of PMMA/POSS. Similarly, PMMA/POSS nanocomposites were characterized in the same way. Based on the data of A_{585}/A_{1731}

in the nanocomposites, the actual amount of POSS incorporated into the nanocomposites were determined and listed in the Table 1.
To further determine the OV-POSS content, the nanocomposites were calcined at 1000°C in air and the obtained silica ceramic yields were used to back calculate the content of POSS according to equation (1).

$$\text{OV-POSS (wt)\%} = W \times \frac{633.0}{60.1 \times 8} \times 100\% \quad (1)$$

where, W represents the silica ceramic yields. The calculated POSS content given by both FTIR and TGA were summarized in Table 1. From the table, it is found that the results are in good agreement. For example, the content ratio of FTIR is 0.11% less than the counterpart of TGA when 15 % POSS were fed. The greatest difference is less than 0.5%, which occurs in the 20 % addition of POSS.

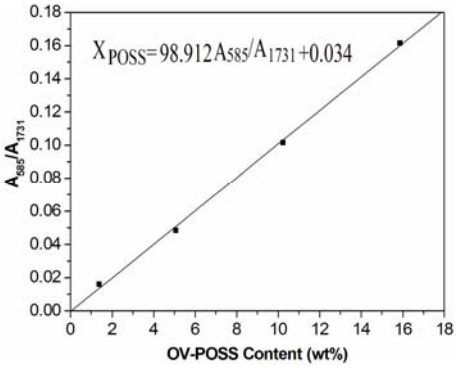

Figure 2. A_{585}/A_{1731} vs. OV-POSS content curve for the blends of PMMA and OV-POSS

Table 1. Effect of POSS contents on the structure of the nanocomposites

No.	OV-POSS content (%)				yield (wt%)	x [a]	M_n ($\times 10^3$ g·mol^{-1})	M_w ($\times 10^3$ g·mol^{-1})	PDI	silica yield (%)[b]
	feed mass ratio	product mass ratio (FTIR)	product mole ratio (FTIR)	product mass ratio (TGA)						
1	0	0	0	0	72.9	0	20.2	39.1	1.94	0
2	1	0.91	0.15	0.96	72.0	0	21.3	39.9	1.87	0.73
3	5	3.84	0.63	4.05	70.6	0.60	26.6	73.8	2.78	3.08
4	10	6.76	1.13	6.81	69.4	2.53	34.5	283.3	8.21	5.17
5	15	12.27	2.16	12.38	63.0	3.78	39.6	275.4	6.96	9.41
6	20	14.06	2.52	14.51	49.3	4.96	38.8	156.6	4.03	11.02

[a] Data calculated based on the product mole ratio (FTIR).
[b] Data determined by TGA at 1000°C in air.

The ^{1}H-NMR spectra of OV-POSS, pure PMMA, and PMMA/OV-POSS nanocomposite are shown in Figure 3(a,b,c). For OV-POSS macromer, the multiplet resonance peaks at about 6.0 ppm are observed because of the coupling of hydrogen protons from the vinyl groups [Figure 3(a)]. In Figure 3(b), methoxyl (OCH_3) protons give a singlet at 3.60 ppm, the peaks in the region between 1.29~2.20 ppm can be assigned to the methylene protons($-CH_2$), the resonances ranging from 0.87 to 1.24 ppm

correspond to the methyl protons (-CH_3) banded with quaternary carbon. After a comparison of Figure 3(b) and 3(c), it can be seen that the ^{1}H NMR spectrum of the PMMA/POSS nanocomposite resembles that of the pure PMMA, except that a new wide resonance around 6.0 ppm appears. From the zoom-in inset (Figure 3(c)), residual peaks can be found in the area of 5.7~6.3 ppm, which belongs to the unreacted vinyl in POSS. This suggests the vinyl groups of the POSS monomer are not consumed completely during the copolymerization. The resonance bands of methylene and methine protons from the reacted vinyl groups of POSS segments overlap with those of methyl and methylene protons in the PMMA from 0.8 to 2.2 ppm.

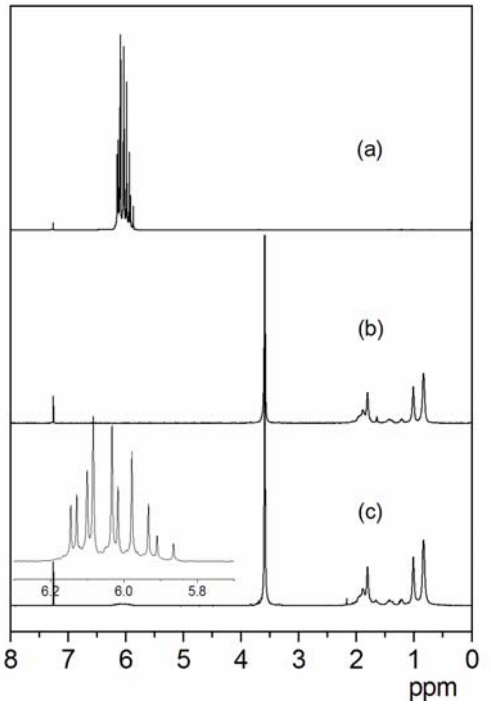

Figure 3. ^{1}H NMR spectra of (a) OV-POSS, (b) pure PMMA, (c) PMMA/OV-POSS nanocomposite containing 12.27 wt% of OV-POSS. The zoom-in inset in (c) is ^{1}H NMR spectra of nanocomposite area from 5.7~6.3ppm

The ^{1}H NMR resonance peaks of CH_2=CH- (in OV-POSS) and -OCH_3 (in PMMA), locating at 6.0 and 3.6 ppm respectively, are not overlapped with each other. Taking into account of the facts that every MMA repeat unit possesses one -OCH_3 group, whereas each vinyl group from OV-POSS has the same number of protons, the relative intensity of above two resonances should be identical. Therefore, we can estimate the number of unreacted vinyl groups (x) from POSS cages based on the relative peak area for vinyl groups and the POSS content in the nanocomposites, which can be expressed as follows:

$$\text{OV-POSS mol\%} = \frac{A_{6.0}/3x}{A_{6.0}/3x + A_{3.6}/3} \times 100\% \qquad (2)$$

where, $A_{6.0}$ and $A_{3.6}$ represent the absorbance peak area at 6.0 and 3.6 ppm, respectively; *x* refers to the average number of unreacted vinyl groups from POSS cages. In terms of the ^{1}H NMR resonance peak areas, the *x* values are calculated and shown in Table 1. The results show that, in average, 3~8 vinyl groups from POSS macromers participated in the copolymerization, and the number of unreacted vinyl groups of OV-POSS increased with the increment of the amount of POSS in the reaction. This change is probably due to steric hindrance of the bulky POSS monomer, resulting in a decrease of the reactivity of MMA monomers.

Swelling experiments in ethyl acetate were performed to investigate the solubility of all samples. Our results indicate that these nanocomposites could dissolve quite well in ethyl acetate, making us believe that the synthesized composites are most likely in star-shaped structure rather than in cross-linked form [33].

Gel permeation chromatography (GPC) was used for determining molecular weights and polydispersity index (PDI) of the nanocomposites and PMMA. The results of GPC analyses are listed in Table 1. The weight-average molecular weights (M_w) of the PMMA is 20.2×10^3 g·mol^{-1} with a polydispersity of 1.94. The M_w values of composites increased upon increasing the OV-POSS contents up to 12.27 wt%. However, as the amount of POSS increased to 14.06 wt%, the molecular weights decreased slightly. We attribute the decreased molecular weights of the composites to the decrease of the activity of MMA monomer due to the steric hindrance of the bulky POSS monomer.

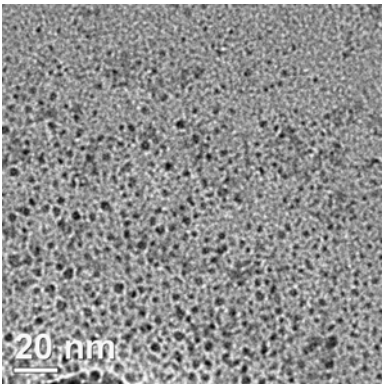

Figure 4. TEM micrograph of the PMMA nanocomposite containing 12.27 wt% of POSS

Figure 4 displays the TEM image of the hybrid poly(methyl methacrylate) composite containing 12.27 wt% of POSS. It can be seen that the black dots (the POSS domains) in Figure 4 represent OV-POSS dispersed at about 1.5-4 nm level, which illustrates that the organic-inorganic PMMA/POSS nanocomposites were obtained using this method.

Thermal Properties

Glass Transition Behavior

DSC curves of the PMMA/OV-POSS nanocomposites with different OV-POSS contents are shown in Figure 5, and the glass transition temperatures (T_g's) are listed in Table 2. All the nanocomposites and the pure PMMA displayed the only glass transition. In compared with pure PMMA, the T_g's of the nanocomposites increased

upon increasing the POSS content up to 12.27 wt %, but then they decreased unexpectedly as loading is more. We also found that the T_g of the PMMA/OV-POSS nanocomposites has been enhanced by 23°C, which is higher than that in Weickmann's study (18°C) [31].

To our knowledge, the factors leading to the variation of T_g of POSS-containing hybrids include POSS species [31], POSS loading [45] and the hybrids structures. In our study, the remarkable T_g improvement of the nanocomposites could be ascribed to the severe hindering effect of POSS, which inhibits the motion of the PMMA chains in the polymeric matrix. In addition, we also considered that the formation of star-shaped structures with cubic silsesquioxane core is propitious to the T_g improvement [42]. However, it is worth noting that the T_g's of the nanocomposites did not monotonically increase with increasing the concentration of POSS, and the maximum T_g value was observed for the composites containing 12.27 wt % of POSS, although all the samples displayed the enhanced T_g's. The T_g depression could be attributed to the increased incorporation of the low molecular weight species [23]. For the nanocomposite with 14.06 wt% of POSS, the greater steric hindrance of the POSS cages tends to increase the "free volume" internally and decrease the reactivity of the MMA monomers, which leads to a relatively larger fractions of low molecular weight components.

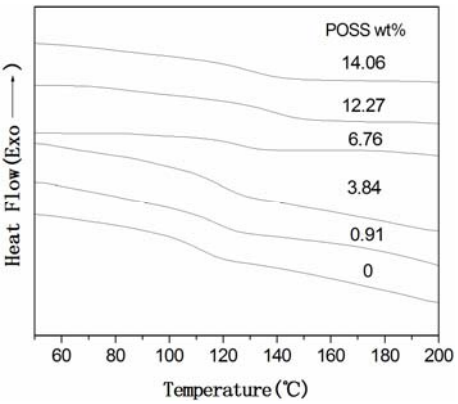

Figure 5. DSC thermograms of pure PMMA and PMMA/OV-POSS nanocomposites

Table 2. Thermal properties of PMMA/OV-POSS nanocomposites

No.	product mass ratio (FTIR) (wt %)	T_g (°C)	T_{dec1} (°C)	T_{dec2} (°C)	char yield (wt %, 600°C)
1	0	109.0	180	210	0
2	0.91	118.6	193	242	1.6
3	3.84	119.6	242	274	3.3
4	6.76	124.0	269	289	8.2
5	12.27	131.9	273	296	11.2
6	14.06	123.6	165	235	13.5

Thermal stability

Figure 6 illustrates the TGA thermograms of the pure PMMA and POSS-containing nanocomposites under nitrogen, the related characteristic data are given in Table 2.

The TGA curve of pure PMMA exhibits three main degradation steps. The first and second steps degradation are due to scission of head-to-head and unsaturated chain ends of the polymer respectively, while the third one is associated with random scission [46]. Unlike the degradation of pure PMMA, the portion of the first and second steps of the POSS/PMMA nanocomposites gradually disappears with increasing the POSS contents (less than 12.27 wt%). More attractively, the T_{dec1} and T_{dec2} (5% and 10% mass loss temperatures) were increased by 93°C and 86°C respectively for samples with the POSS loading ranging from 0 to 12.27 wt %. These results strongly support that the incorporated POSS retards the scission of head-to-head linkage and vinylidene chain-end initiation. However, as the amount of the POSS increased to 14.06 wt%, the thermal stability decreased markedly. The decrease of T_{dec} may be related to the formation of MMA oligomers and lower molecular weight PMMA chains. In addition, The residual char yields increase with increasing POSS content as expected. All these facts indicated that the thermal stabilities of nanocomposites were significantly enhanced with increasing the inorganic component.

In the present case, it is noted that the thermal stability of PMMA has been improved by 93°C, which is almost double to that in Toepfer's work (43°C) [33]. We proposed two reasons for this significant enhancement. One is that the rigid OV-POSS molecules were covalently bonded with PMMA chains and the nanoscale dispersion of POSS cages in the polymer matrix. The other is that cubic-cage-structured OV-POSS expands the space between PMMA chains, which gives rise to lower thermal conductivity [47].

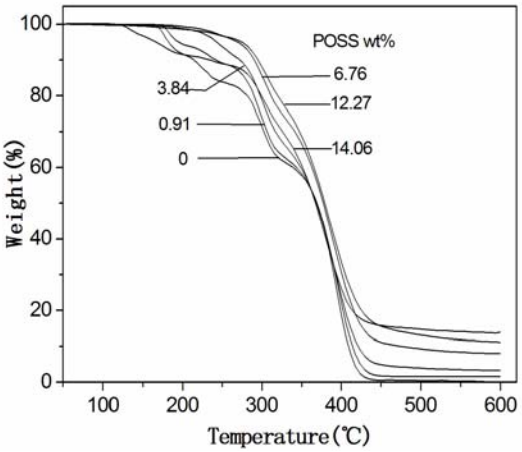

Figure 6. TGA thermograms of pure PMMA and PMMA/OV-POSS nanocomposites

Conclusions

In this work, the nanoscaled well-defined octavinyl-polyhedral oligomeric silsesquioxane was synthesized and employed to prepare POSS-containing poly(methyl methacrylate) nanocomposites. The actual amount of POSS incorporated into the nanocomposites and the reaction degree of vinyl groups in the POSS were

estimated by FTIR, TGA and NMR. The DSC and TGA confirm unambiguously that the enhancement in the thermal properties largely depended on the POSS concentration. As the OV-POSS loading increased from 0 to 12.27 wt%, the values of glass transition temperature (T_g) and thermal decomposition temperature (T_{dec1}) of the nanocomposite were enhanced by 23°C and 93°C, respectively. All our experimental data support the existence of the reinforcement effect at molecular level of the POSS cages on the PMMA matrix and the formation of the star-shaped structures with cubic silsesquioxane core in our system.

Acknowledgements. The authors wish to acknowledge the National Natural Science Fund of China (No. 50572039) and R&D Fund from University in Jiangsu Province (JHB06-04) for support of this work.

References

1. Whitesides GM, Mathias JP, Seto CT (1991) Science 254:1312
2. Tsuchida A, Bolln C, Sernetz FG, Frey H, Mulhaupt R (1997) Macromolecules 30:2818
3. Priya L, Jog JP (2002) J Polym Sci Part B Polym Phys 40:1682
4. Burnside SD, Giannelis EP (1995) Chem Mater 7:1597
5. Wang YZ, Zhang LQ, Tang CH, Yu DS (2000) J Appl Polym Sci 78:1879
6. Gangun S, Dean D (2003) Polymer 44:1315
7. Rehman HU, Sarwar MI, Ahmad Z, Krug H, Schmidt H (1997) J Non-Cryst Solids 211:105
8. Dufresne A, Paillet M, Putaux JL, Canet R, Carmona F (2002) J Mater Sci 37:3915
9. Pandey JK, Reddy KR, Kumar AP, Singh RP (2005) Polym Degrad Stab 88:234
10. Zanetti M, Camino G, Canavese D, Morgan AB, Lamelas FJ, Wilkie CA (2002) Chem Mater 14:189
11. Dodiuk H, Belinski I, Dotan A, Kenig S (2006) J Adhes Sci Technol 20:1345
12. Barrau S, Demont P, Perez E, Peigney A, Laurent C, Lacabanne C (2003) Macromolecules 36:9678
13. Xu HY, Kuo SW, Lee JY, Chang FC (2000) Polymer 43:5117
14. Lee Y, Kuo SW, Su YC, Chen JK, Tu CW, Chang FC (2004) Polymer 45:6321
15. Jash P, Wilkie CA (2005) Polym Degrad and Stab 88:401
16. Huang JC, He CB, Xiao Y, Mya KY, Dai J, Siow YP (2003) Polymer 44:4491
17. Choi J, Harcup J, Yee AF, Zhu Q, Laine RM (2001) J Am Chem Soc 123:11420
18. Dodiuk H, Kenig S, Blinsky I, Dotan A, Buchman A (2005) Int J Adhes Adhes 25:211
19. Dodiuk-Kenig H, Maoz Y, Lizenboim K, Eppelbaum I, Zalsman B, Kenig S (2006) J Adhes Sci Technol 20:1401
20. Dodiuk H, Rios PF, Dotan A, Kenig S (2007) Polym Advan Technol 18:746
21. Efrat T, Dodiuk H, Kenig S, Mccarthy S (2006) J Adhes Sci Technol 20:1413
22. Li G, Wang L, Ni H, Pittman J CU (2001) J Inorg Organomet Polym 11:123
23. Lin HC, Kuo SW, Huang CF, Chang F (2006) Macromol Rapid Commun 27:537
24. Choi J, Yee AF, Laine RM (2003) Macromolecules 36:5666
25. Fina A, Abbenhuis HCL (2006) Polym Degrad and Stab 91:2275
26. Hong RY, Fu HP, Zhang YJ, Liu L, Wang J, Li HZ, Zheng Y (2007) J Appl Polym Sci 105:2176
27. Džunuzović E, Jeremić K, Nedeljković JM (2007) Eur Polym J 43: 3719
28. Wang H, Xu P, Zhong W, Shen L, Du Q (2005) Polym Degrad Stab 87:319
29. Kopesky ET, Haddad TS, Gareth HM, Robert EC (2005) Polymer 46:4743
30. Kopesky ET, Gareth HM, Robert EC (2006) Polymer 47:299
31. Weickmann H, Delto R, Thomann R, Brenn R, Döll W, Mülhaupt R (2007) J Mater Sci 42:87

32. Kopesky ET, Haddad TS, Robert EC, Gareth HM (2004) Macromolecules 37:8992
33. Toepfer O, Neumann D, Choudhury NR, Whittaker A, Matisons J (2005) Chem Mater 17:1027
34. Zou Q, Zhang S, Tang Q, Wang S, Wu L (2006) Journal of Chromatography A 1110:140
35. Zou Q, Zhang S, Wang S, Wu L (2006) Journal of Chromatography A 1129:255
36. Amir N, Levina A, Silverstein MS (2007) J Polym Sci Part A Polym Chem 45:4264
37. Zhang W, Fu BX, Seo Y, Schrag E, Hsiao B, Mather PT, Yang NL, Xu D, Ade H, Rafailovich M, Sokolov J (2002) Macromolecules 35:8029
38. Koh K, Sugiyama S, Morinaga T, Ohno K, Tsujii Y, Fukuda T, Yamahiro M, Iijima T, Oikawa H, Watanabe K, Miyashita T (2005) Macromolecules 38:1264
39. Costa RR, Vasconcelos WL, Tamaki R, Laine RM (2001) Macromolecules 34:5398
40. Ohno K, Sugiyama S, Koh K, Tsujii Y, Fukuda T, Yamahiro M, Oikawa H, Yamamoto Y, Ootake N, Watanabe K (2004) Macromolecules 37:8517
41. Romo-Uribe A, Mather PT, Haddad TS, Lichtenhan J D (1998) J Polym Sci Part B Polym Phys 36:1857
42. Xu H, Yang B, Wang J, Guang S, Li C (2005) Macromolecules 38:10455
43. Xu H, Yang B, Gao X, Li C, Guang S (2006) J Appl Poly Sci 101:3730
44. Tang BZ, Xu HY, Lee WYJ, Lee PSP, Xu K, Sun Q, Cheuk KKL (2000) Chem Mater 12:1446
45. Mather PT, Jeon HG, Romo-Uribe A, Haddad TS, Lichtenhan JD (1999) Macromolecules 32:1194
46. Kashiwagi T, Inaba A, Brown JE (1986) Macromolecules 19: 2160
47. Liu H, Zheng S, Nie K (2005) Macromolecules 38:5088